Revue des Composites et des Matériaux Avancés-Journal of Composite and Advanced Materials
Vol. 36, No. 4, August, 2026, pp. 833-840
Journal homepage: http://iieta.org/journals/rcma

Effect of Octadecanethiol Treatment on Wettability, Fracture Morphology, and Mechanical Properties of Soybean Hull-Derived Cellulose/Epoxy Composites

Arya Mahendra Sakti[1*], Dewi Puspitasari[1], Andita Nataria Fitri Ganda[1], Femiana Gapsari[2], Diah Wulandar[1], Aji Nugroho[1], Dyah Riandadari[1], Firman Yasa Utama[1], Muhammad Mukid Almudakir[1], Aprilia Setya Femina[3]

[1] Mechanical Engineering Department, Universitas Negeri Surabaya, Surabaya 60231, Indonesia
[2] Mechanical Engineering Department, Brawijaya University, Malang 65145, Indonesia
[3] Nutrition Department, Universitas Negeri Surabaya, Surabaya 60231, Indonesia

Corresponding Author Email: aryamahendra@unesa.ac.id

https://doi.org/10.18280/rcma.360412

Received: 12 June 2026
Revised: 6 August 2026
Accepted: 18 August 2026
Available online: 31 August 2026

Keywords:
epoxy composite, soybean hull-derived cellulose, octadecanethiol, water contact angle, fracture morphology, mechanical properties

ABSTRACT

Soybean hull is a lignocellulosic agro-industrial by-product that can be valorized as a cellulose-rich reinforcement; however, its surface characteristics may limit compatibility with polymer matrices. This study evaluated octadecanethiol (ODT) treatment of soybean hull-derived cellulose (SHC) using treatment solutions containing 10%, 20%, and 30% ODT (v/v). The composites were fabricated at a fixed nominal SHC-to-epoxy volume ratio of 60:40, corresponding to 60 vol% SHC reinforcement and 40 vol% epoxy matrix. Tensile strength, flexural strength, Shore D hardness, Charpy-type impact strength, apparent epoxy-resin contact angle, and fracture-surface morphology were evaluated. Mechanical properties were determined from five independent specimens per condition (n = 5) and are reported as mean ± standard deviation. K-ODT30 exhibited the highest mean mechanical properties, with a tensile strength of 44.70 ± 1.70 MPa, flexural strength of 78.10 ± 2.50 MPa, Shore D hardness of 81.20 ± 1.00, and impact strength of 19.70 ± 0.70 kJ/m². The apparent epoxy-resin contact angle increased progressively from 50.4° for K0 to 93.8° for K-ODT30, indicating reduced spreading of uncured epoxy on the ODT-treated SHC surface. Scanning Electron Microscopy (SEM) observations showed cavity- or void-like regions and exposed rough surfaces in K0, whereas K-ODT30 exhibited a more continuous striated fracture-surface morphology. Overall, increasing ODT concentration up to 30% (v/v) was associated with higher mean mechanical properties and pronounced changes in the apparent epoxy-wetting behavior and fracture morphology of SHC/epoxy composites.

1. INTRODUCTION

Natural fiber-reinforced polymer composites are increasingly investigated for lightweight structures in which renewable reinforcement, low density, and waste valorization are desirable. Their engineering performance, however, depends strongly on reinforcement morphology, matrix selection, processing quality, and moisture sensitivity rather than on fiber origin alone [1-4].

Soybean hull is an abundant lignocellulosic residue from soybean processing and is a relevant source of cellulose-rich material. Published soybean-hull studies report substantial cellulose content and demonstrate that alkaline pulping, bleaching, and related treatments can isolate cellulose-rich fractions suitable for higher-value materials [5, 6]. This composition supports its use as a precursor for composite reinforcement rather than only as a low-value residue [7].

Previous work has already established the feasibility of soybean-derived reinforcement in polymer systems. Balla et al. [8] showed that chemically modified soybean-hull fibers could reduce porosity and improve the mechanical response of fused-filament-fabricated thermoplastic copolyester composites. Related studies by the present research group characterized soybean-derived fibers and examined alkali/ZnO-based surface modification [9, 10]. These studies provide a material basis for soybean-derived reinforcement, but they do not resolve the behavior of a cellulose-rich soybean-hull fraction in an epoxy thermoset.

A central challenge in lignocellulosic/epoxy systems is the mismatch between the hydrophilic, hydroxyl-rich reinforcement surface and the comparatively less polar cured matrix. This mismatch can contribute to incomplete wetting, interfacial gaps, moisture uptake, and inefficient stress transfer [11-16]. Surface modification is therefore commonly used to alter surface chemistry and roughness; nevertheless, composite properties can also be controlled by dispersion, orientation, porosity, reinforcement dimensions, residual moisture, and cure quality [11, 13-18].

Direct evaluation of an interface requires more than bulk mechanical data. Single-fiber or yarn pull-out measurements, for example, can quantify interfacial shear strength and distinguish interface performance from changes in the matrix or reinforcement [12, 19]. Accordingly, tensile, flexural, hardness, impact, contact-angle, and Scanning Electron Microscopy (SEM) results in the present study are interpreted as complementary composite-level observations rather than as direct measurements of interfacial bond strength.

Epoxy was selected as the matrix because it can be processed and cured at relatively low temperatures while providing useful mechanical performance and dimensional stability for laboratory composite evaluation. For lignocellulosic reinforcement, low-temperature curing is advantageous because excessive thermal exposure can accelerate moisture loss, degradation, or changes in fiber structure. Even with epoxy, however, final properties remain sensitive to resin-to-hardener ratio, void content, reinforcement distribution, and cure history [12, 14, 15, 17, 20].

Octadecanethiol (ODT) contains a thiol head group and a nonpolar C18 hydrocarbon chain. ODT is well known to form ordered hydrophobic layers on suitable reactive inorganic surfaces [21]. In cellulose-based materials, Lin et al. [22] used an anchoring MPTES/POSS chemistry before introducing ODT to cotton, obtaining a highly hydrophobic surface. That precedent supports the hydrophobic role of long C18 functionality, but it does not demonstrate that ODT forms a specific covalent, ether, or hydrogen-bonded attachment directly to the soybean hull-derived cellulose (SHC) surface used here.

The unresolved question is therefore whether increasing nominal ODT treatment level is associated with measurable changes in apparent water wettability, fracture morphology, and bulk mechanical response in a SHC/epoxy composite. This distinction is important because changes in water contact angle may correlate with surface modification while remaining insufficient, by themselves, to prove epoxy wetting, work of adhesion, or chemical bonding.

Accordingly, this study evaluates SHC/epoxy composites fabricated at a fixed nominal SHC-to-epoxy volume ratio of 60:40, corresponding to 60 vol% SHC reinforcement and 40 vol% epoxy matrix. SHC was treated using ODT solutions at concentrations of 10%, 20%, and 30% (v/v), together with an untreated control. The effects of ODT treatment were evaluated through tensile strength, flexural strength, Shore D hardness, Charpy-type impact strength, apparent epoxy-resin contact angle, and fracture-surface SEM observations. By relating ODT concentration to mechanical performance, epoxy-wetting behavior, and fracture morphology, this study provides an experimental basis for understanding the role of surface modification in SHC/epoxy composites and supports the future development of more sustainable and resource-efficient composite materials.

2. MATERIAL AND METHODS

2.1 Fiber extraction and octadecanethiol treatment

Soybean hull fiber extraction was carried out through three chemical treatment stages: alkali treatment, bleaching, and hydrolysis. Alkali treatment, or delignification, was performed using a 10% NaOH solution. A 20 g quantity of soybean hull powder was placed in a beaker containing 500 mL of 10% NaOH solution and heated on a hot plate for 1 h at 90–100 °C. After heating, the pretreated material was washed with distilled water until the solution reached neutral pH. The sample was then oven-dried at 100 °C until its moisture content reached approximately 10%. The next stage was bleaching using a 30% H_2O_2 solution to remove residual lignin, coloring substances, and non-cellulosic components remaining after alkali treatment. After bleaching, the sample was washed again with distilled water to neutral pH and dried at 100 °C until the moisture content reached approximately 10%. The third stage was hydrolysis using 5 M H_2SO_4 solution. The previously treated soybean hull powder was heated in 5 M H_2SO_4 for 1 h on a hot plate at 50 °C. After hydrolysis, the sample was washed with distilled water until neutral pH was achieved.

ODT treatment was conducted using ODT solutions prepared in *n*-hexane at concentrations of 10%, 20%, and 30% (v/v), where the stated percentages represent the volumetric fraction of ODT in the treatment solution. The 10%, 20%, and 30% (v/v) solutions were prepared by measuring 10, 20, and 30 mL of ODT, respectively, followed by the addition of *n*-hexane to a final volume of 100 mL. All treatment solutions were freshly prepared immediately before use. Oven-dried SHC was then immersed in the corresponding ODT solution at a liquid-to-solid ratio of 10 mL g^{-1} dry SHC and treated for 60 min at 35 ± 2 °C under continuous magnetic stirring at approximately 300 rpm without ultrasonication. After treatment, the SHC was separated from the solution and rinsed twice with fresh *n*-hexane to remove residual unbound ODT from the particle surfaces. The treated SHC was subsequently oven-dried at 60 °C for 12 h to remove residual solvent before composite fabrication. The untreated control (K0) underwent the same solvent-contact, rinsing, and drying procedures using *n*-hexane without ODT, thereby allowing differences in the resulting composite properties to be primarily attributed to the ODT concentration applied during SHC surface treatment. The nominal formulations are presented in Table 1. ODT percentages represent the volumetric concentration of ODT in *n*-hexane treatment solutions, whereas composite composition is expressed independently as the nominal volume fraction of SHC and epoxy.

2.2 Composite fabrication

The composites were fabricated using a hand lay-up technique followed by light compression molding. The composite formulation was maintained at a nominal SHC-to-epoxy volume ratio of 60:40, corresponding to 60 vol% SHC as the reinforcing phase and 40 vol% epoxy as the matrix. The SHC reinforcement was used in the form of powder or short fibrous particles and was sieved to obtain a particle-size range of approximately 150–250 μm. SHC and epoxy were mechanically mixed for 10 min to obtain a homogeneous mixture, which was subsequently transferred into specimen molds corresponding to the required testing geometries shown in Figure 1. The filled molds were subjected to a compressive pressure of approximately 0.5 MPa for 10 min at room temperature to promote consolidation, reduce void formation, and facilitate matrix distribution throughout the SHC reinforcement. The specimens were initially cured at room temperature for 24 h and subsequently post-cured at 40 °C for 2 h before mechanical testing and characterization.

Table 1. Nominal formulations of soybean hull-derived cellulose (SHC)/epoxy composites

Code	SHC Treatment	Epoxy Volume Fraction	SHC Volume Fraction
K0	Untreated	40 vol%	60 vol%
K-ODT10	ODT 10 % (v/v)	40 vol%	60 vol%
K-ODT20	ODT 20 % (v/v)	40 vol%	60 vol%
K-ODT30	ODT 30 % (v/v)	40 vol%	60 vol%

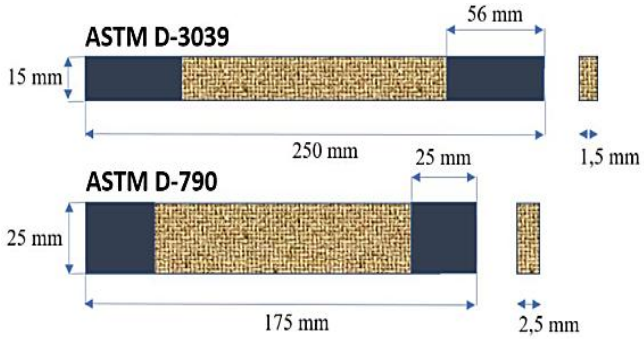

Figure 1. Mechanical-test specimen dimensions used in this study based on available records

2.3 Tensile and flexural testing

Tensile and flexural tests were performed using a TARNO GROCKI UPH universal testing machine with a maximum load capacity of 100 kN. Tensile testing was conducted at a crosshead speed of 2 mm/min. The tensile specimens were rectangular coupons measuring 250 mm in length, 15 mm in width, and approximately 1.5 mm in thickness, with 56-mm-long end tabs attached at both ends in accordance with ASTM D3039 [23]. Tensile strength was calculated as the ratio of the maximum load sustained by the specimen (P) to its initial cross-sectional area (A) and was expressed in N/mm² or MPa. Flexural testing was performed using a three-point bending configuration in accordance with ASTM D790 [24]. The flexural specimens measured 175 mm in length, 25 mm in width, and approximately 2.5 mm in thickness. The tests were conducted at a crosshead speed of 2 mm/min with a support span of 60 mm. The flexural strength of the composites was calculated using Eq. (1), where σb denotes the flexural strength (MPa), P is the maximum applied load (N), L is the support span (mm), B is the specimen width (mm), and H is the specimen thickness (mm) [24].

$$\sigma b = \frac{3.P.L}{2.B.H^2} \quad (1)$$

2.4 Shore D hardness test

Hardness testing was performed according to ASTM D2240 using the Shore D method [25]. The composite specimens had a thickness of 3 mm, width of 15 mm, and length of 35 mm. Testing was carried out at room temperature, approximately 25 °C, using a GS-720N Teclock durometer manufactured in Japan, with a penetration load of 5 kg, equivalent to 49 N. Hardness was measured at five different points on the specimen surface. Each point was recorded at 1 s and 10 s, and the mean value was used as the final composite hardness [25].

2.5 Impact test

Charpy-type impact testing was performed using V-notched specimens measuring 55 mm × 10 mm × 10 mm (length × width × thickness). Each specimen was positioned horizontally on the supports, with the V-notch oriented opposite to the direction of impact. The impact load was applied using an 8.3 kg pendulum, with ASTM D6110 [26] used as a reference for the test equipment and configuration. The energy absorbed by the specimen during fracture was determined from the difference between the pendulum energy measured after impact and the reference energy obtained without a specimen. The impact strength was then calculated by dividing the absorbed energy by the fractured cross-sectional area, as expressed in Eq. (2). In this equation, *Is* represents the impact strength (J/mm²), *Es* is the energy measured after impact (J), *Eo* is the reference energy measured without a specimen (J), and *A* is the fractured cross-sectional area of the specimen (mm²) [26].

$$Is = \frac{Es - Eo}{A} \quad (2)$$

2.6 Wettability

The wettability of the SHC surface by the epoxy matrix was evaluated through static contact-angle measurements using uncured epoxy resin as the probe liquid, following the sessile-drop approach described in ASTM D7334-08 [27], as illustrated in Figure 2. Prior to measurement, the SHC surfaces were cleaned, dried at room temperature, and securely positioned on a specimen holder to permit clear observation of the droplet profile. A 5 µL droplet of epoxy resin was deposited directly onto the SHC surface. For each treatment condition, measurements were conducted at five different surface locations at 25 ± 2 °C, and droplet-profile images were recorded approximately 10 s after deposition. The profiles were captured using a microscope or digital camera coupled with image-analysis software. The apparent contact angle was defined as the angle between the tangent to the epoxy droplet at the three-phase contact line and the SHC surface. A lower contact angle indicates greater spreading of the epoxy resin and therefore higher apparent wettability, whereas a higher contact angle indicates reduced epoxy spreading and lower apparent wettability. The measurements were used to evaluate changes in the interaction between the SHC surface and uncured epoxy resin following ODT treatment [27].

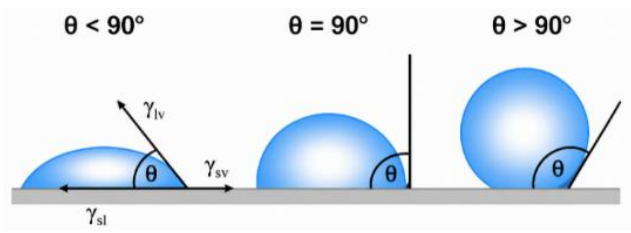

Figure 2. Schematic illustration of the apparent contact angle formed between an uncured epoxy-resin droplet and the soybean hull-derived cellulose (SHC) surface, based on the sessile-drop method described in ASTM D7334-08 [27]

3. RESULTS AND DISCUSSION

3.1 Mechanical properties

Figure 3 summarizes the tensile strength, flexural strength, Shore D hardness, and Charpy-type impact strength of the untreated and ODT-treated SHC/epoxy composites. The mechanical properties are reported as mean ± SD from five independent specimens for each condition (n = 5). All four mechanical properties increased progressively with increasing ODT concentration, with K-ODT30 exhibiting the highest mean values among the investigated formulations. Nevertheless, the magnitude of the incremental improvement decreased between K-ODT20 and K-ODT30.

The tensile strength increased from 31.20 ± 1.50 MPa for K0 to 40.60 ± 1.80 MPa for K-ODT10, 43.20 ± 1.60 MPa for K-ODT20, and 44.70 ± 1.70 MPa for K-ODT30. Relative to the untreated composite, these values correspond to increases of 30.13%, 38.46%, and 43.27%, respectively. The largest improvement occurred between K0 and K-ODT10, whereas increasing the ODT concentration from 20% to 30% resulted in a further increase of only 3.47%. The results therefore demonstrate a progressive but diminishing tensile-strength response as the ODT concentration increased. Because composite tensile behavior is governed not only by interfacial interactions but also by reinforcement distribution, matrix continuity, porosity, and processing quality, the observed improvements should be interpreted as composite-level responses rather than direct evidence of increased interfacial bond strength [12, 14, 19].

Flexural strength followed a similar trend, increasing from 58.40 ± 2.10 MPa for K0 to 69.20 ± 2.40 MPa for K-ODT10, 74.90 ± 2.30 MPa for K-ODT20, and 78.10 ± 2.50 MPa for K-ODT30. These values represent increases of 18.49%, 28.25%, and 33.73%, respectively, relative to K0. The additional increase between K-ODT20 and K-ODT30 was 4.27%, again indicating a smaller incremental response at the highest ODT concentration. Because three-point bending generates tensile, compressive, and shear stresses simultaneously, flexural performance reflects the combined effects of matrix continuity, reinforcement distribution, structural defects, and stress transfer within the composite [12, 19, 28].

Shore D hardness increased from 74.00 ± 1.00 for K0 to 77.10 ± 0.90 for K-ODT10, 79.60 ± 1.10 for K-ODT20, and 81.20 ± 1.00 for K-ODT30. Relative to K0, the increases were 4.19%, 7.57%, and 9.73%, respectively. Although the relative changes were smaller than those observed for tensile, flexural, and impact strength, the consistent increase indicates greater resistance to localized surface indentation in the ODT-treated composites.

Charpy-type impact strength increased from 14.60 ± 0.80 kJ/m² for K0 to 17.40 ± 0.90 kJ/m² for K-ODT10, 19.10 ± 0.80 kJ/m² for K-ODT20, and 19.70 ± 0.70 kJ/m² for K-ODT30. These increases correspond to 19.18%, 30.82%, and 34.93%, respectively, relative to K0. The comparatively small increase of 3.14% from K-ODT20 to K-ODT30 indicates that the impact response also tended toward a plateau at higher ODT concentrations. The higher values indicate increased energy absorption prior to fracture under the Charpy-type loading configuration; however, the response may reflect several interacting mechanisms, including crack propagation, matrix fracture, reinforcement pull-out, void distribution, and interfacial debonding [12, 29].

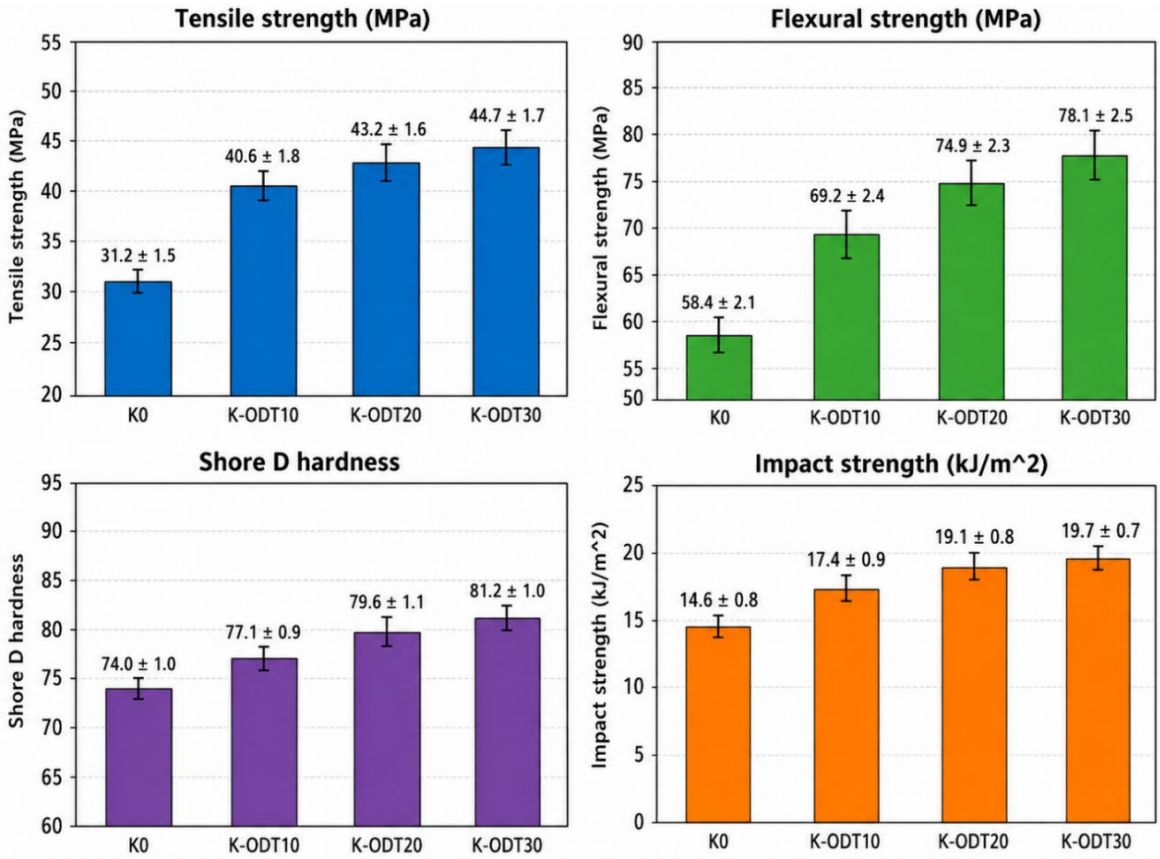

Figure 3. Mechanical properties of the composites shown as mean values only: (a) tensile strength, (b) flexural strength, (c) Shore D hardness, and (d) Charpy-type impact strength

The mechanical performance of K-ODT30 was further compared with selected natural-fiber/epoxy systems reported in the literature (Table 2). Its tensile strength of 44.70 MPa was comparable to the 45.0 MPa reported for plasma-treated bamboo cellulose/epoxy composites [20], exceeded the 32.84 MPa reported for NaOH-treated Moonj-fiber/epoxy composites [30], and remained below the 66.90 MPa obtained for alkali-treated areca sheath/epoxy composites [31]. The flexural strength of K-ODT30 (78.10 MPa) was higher than that of the plasma-treated bamboo cellulose/epoxy system (49.2 MPa) [20] and approached those reported for areca sheath/epoxy (80.17 MPa) and Moonj/epoxy composites (82.5 MPa) [31]. These comparisons provide an engineering context rather than a direct performance ranking because reinforcement fraction, matrix composition, surface treatment, reinforcement morphology, processing conditions, and testing procedures differ among studies.

Table 2. Engineering context for selected natural-fiber/epoxy composites from recent literature

Composite System/Condition	Tensile (MPa)	Flexural (MPa)
Present SHC/epoxy; K-ODT30; nominal 60 wt% SHC	44.70	78.10
Bamboo cellulose/epoxy; 30 min Ar plasma [20]	45.0	49.2
Areca sheath/epoxy; 5% alkali; 30 vol%; 15 mm [31]	66.90	80.17
Moonj/epoxy; 3% NaOH; 40% fiber [30]	32.84	82.5
Agel leaf/epoxy + carbon; VAPRI; 40% ALF [28]	128.51	238.51

Note: Soybean hull-derived cellulose (SHC), octadecanethiol (ODT), agel leaf fiber (ALF).

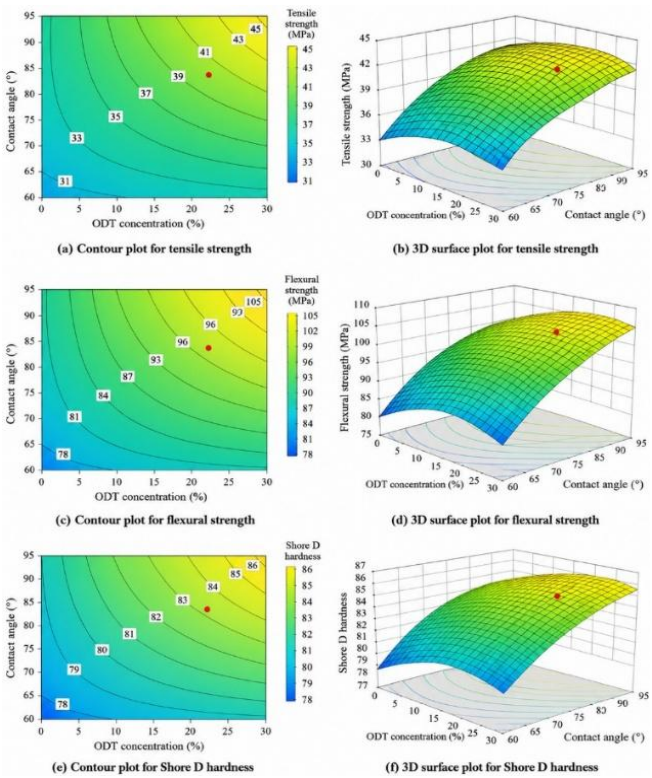

Figure 4. Descriptive contour and three-dimensional surface plots illustrating the relationships among octadecanethiol (ODT) concentration, apparent epoxy-resin contact angle, and mean mechanical properties of soybean hull-derived cellulose (SHC)/epoxy composites

Figure 4 provides descriptive contour and three-dimensional surface visualizations of the relationships among ODT concentration, apparent epoxy-resin contact angle, and mean mechanical responses. These interpolated surfaces are intended only to illustrate the experimentally observed trends across the four formulations and should not be interpreted as statistically fitted or predictive response-surface models.

3.2 Wettability

The apparent epoxy-resin contact angle increased systematically with increasing ODT concentration, from 50.4° for K0 to 64.8° for K-ODT10, 88.4° for K-ODT20, and 93.8° for K-ODT30 (Figure 5). Thus, increasing the ODT concentration from 0% to 30% produced an overall increase of 43.4° in the apparent contact angle. K0 exhibited the greatest spreading of the uncured epoxy resin, whereas K-ODT30 showed the lowest degree of spreading.

Because epoxy resin was used directly as the probe liquid, an increasing contact angle represents lower apparent epoxy wettability, rather than increased wettability. The contact-angle trend therefore indicates that ODT treatment progressively modified the SHC surface in a manner that reduced the spreading of uncured epoxy resin. Importantly, the simultaneous increases in apparent epoxy-resin contact angle and mechanical performance demonstrate that the higher mechanical properties cannot be explained simply by enhanced macroscopic resin spreading over the treated SHC surface.

This apparently contrasting behavior may reflect the complexity of wetting and interfacial phenomena in heterogeneous lignocellulosic composites. Contact-angle measurements are influenced by surface chemistry, roughness, porosity, liquid viscosity, penetration into surface irregularities, and measurement time [27, 32]. Consequently, the measured contact angle represents an apparent macroscopic wetting response rather than a direct measure of interfacial adhesion. In addition, measurements using a single probe liquid are insufficient to determine surface free energy, work of adhesion, or specific polar and dispersive interactions. Direct interfacial shear testing and complementary surface-chemical characterization would therefore be required to establish the mechanism responsible for the mechanical changes [11, 12, 33].

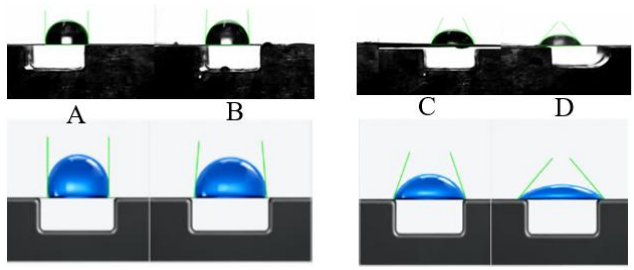

Figure 5. Apparent epoxy-resin contact-angle images for (a) K0, (b) K-ODT10, (c) K-ODT20, and (d) K-ODT30
Note: Octadecanethiol (ODT).

3.3 Fracture-surface morphology

Representative SEM fracture surfaces of K0 and K-ODT30 are compared in Figure 6. The untreated K0 composite exhibited irregular cavity- or void-like regions together with rough, locally exposed surface features. In contrast, K-ODT30

showed a more continuous fracture surface characterized by pronounced striated regions and greater apparent matrix/residue coverage within the observed area [34, 35].

These morphological differences accompanied the changes in mechanical performance. K-ODT30 exhibited the highest tensile strength (44.70 ± 1.70 MPa), flexural strength (78.10 ± 2.50 MPa), Shore D hardness (81.20 ± 1.00), and impact strength (19.70 ± 0.70 kJ/m²), whereas K0 showed consistently lower mechanical values and a fracture surface containing more prominent cavity-like discontinuities. The combined observations indicate that ODT treatment was associated with changes in both fracture morphology and bulk mechanical response.

Nevertheless, the SEM observations provide qualitative rather than quantitative evidence. Representative micrographs were available only for K0 and K-ODT30, and parameters such as void-area fraction, particle pull-out density, crack density, reinforcement dispersion, and interfacial-gap dimensions were not quantitatively determined. Therefore, the SEM images should not be considered direct evidence of stronger chemical bonding or quantified interfacial adhesion. Further quantitative image analysis, direct interfacial testing, and surface-chemical characterization would be required to establish a mechanistic relationship between ODT treatment, fracture morphology, and mechanical performance [11, 12, 19].

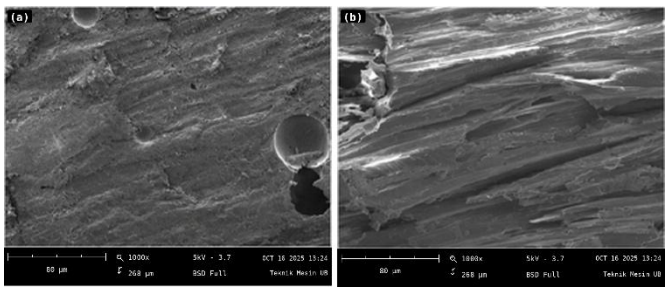

Figure 6. Representative SEM fracture-surface morphologies of (a) untreated K0 and (b) K-ODT30 soybean hull-derived cellulose (SHC)/epoxy composites
Note: Scanning Electron Microscopy (SEM), octadecanethiol (ODT).

4. CONCLUSION

This study demonstrated that ODT treatment was associated with systematic changes in the mechanical response, apparent epoxy-resin wettability, and fracture morphology of SHC/epoxy composites fabricated at a fixed nominal composition of 60 vol% SHC and 40 vol% epoxy. Among the investigated formulations, K-ODT30 produced the highest mean tensile strength (44.70 ± 1.70 MPa), flexural strength (78.10 ± 2.50 MPa), Shore D hardness (81.20 ± 1.00), and Charpy-type impact strength (19.70 ± 0.70 kJ/m²), corresponding to increases of 43.27%, 33.73%, 9.73%, and 34.93%, respectively, relative to untreated K0. The apparent epoxy-resin contact angle simultaneously increased from 50.4° for K0 to 93.8° for K-ODT30, indicating progressively reduced spreading of uncured epoxy resin on the ODT-treated SHC surface. This finding shows that the improvement in bulk mechanical performance cannot be attributed solely to enhanced macroscopic epoxy wettability. Qualitative SEM observations further revealed a transition from cavity- and void-like features in K0 toward a more continuous striated fracture-surface morphology in K-ODT30. Overall, K-ODT30 exhibited the highest mean mechanical performance within the investigated concentration range, although direct interfacial and surface-chemical analyses remain necessary to establish the underlying reinforcement–matrix interaction mechanisms.

ACKNOWLEDGMENT

The authors sincerely appreciate the Department of Mechanical Engineering, Faculty of Vocational Studies, Universitas Negeri Surabaya, for providing academic support and research facilities throughout this study. The authors also gratefully acknowledge the laboratory staff and all individuals who contributed to specimen preparation, testing, and characterization. Their technical support and constructive input were valuable to the completion of this research.

REFERENCES

[1] Kurniasih, P., Wirawan, W.A., Narto, A., et al. (2023). Flammability and morphology of Agel leaf fibre-epoxy composite modified with carbon powder for fishing boat applications. Archives of Materials Science and Engineering, 122(1): 13-21. https://doi.org/10.5604/01.3001.0053.8842

[2] Eguchi, H., Yasui, Y., Nagata, K. (2025). Bio-based composites reinforced with surface-modified cellulose nanofiber scaffolds: Influence of interfacial compatibility on surface mechanical properties. Journal of Fiber Science and Technology, 81(12): 208-214. https://doi.org/10.2115/fiberst.2025-0029

[3] Mousa, S.A., Siddiqui, V.U., Hamidy, A.N.B.M., et al. (2026). A review of date palm fiber composites: Processing, properties, applications, and challenges. Journal of Natural Fibers, 23(1): 2617371. https://doi.org/10.1080/15440478.2026.2617371

[4] Azriena, H.A.A., Ilyas, R.A., Kamaruddin, Z.H., et al. (2025). Recent developments in lignocellulosic banana (Musa spp.) fiber-based biocomposites and their potential industrial applications: A comprehensive review. International Journal of Biological Macromolecules, 323: 147180. https://doi.org/10.1016/j.ijbiomac.2025.147180

[5] Robles Barros, P.J., Ramirez Ascheri, D.P., Santos, M.L.S., et al. (2020). Soybean hulls: Optimization of the pulping and bleaching processes and carboxymethyl cellulose synthesis. International Journal of Biological Macromolecules, 144: 208-218. https://doi.org/10.1016/j.ijbiomac.2019.12.074

[6] Moramarco, A., Ricca, E., Acciardo, E., Laurenti, E., Bracco, P. (2025). Cellulose extraction from soybean hulls and hemp waste by alkaline and acidic treatments: An in-depth investigation on the effects of the chemical treatments on biomass. Polymers, 17(9): 1220. https://doi.org/10.3390/polym17091220

[7] Zeng, X., Jia, Z., Zhayitijiang, Z., Ma, B., Zou, X. (2026). Application of octenylsuccinic anhydride-modified soybean hull nanocellulose for synergistic reinforcement of PVA composite films in beef preservation. Journal of Food Measurement and Characterization, 20: 11148-11161. https://doi.org/10.1007/s11694-026-04363-1

[8] Balla, V.K., Tadimeti, J.G.D., Kate, K.H., Satyavolu, J.

(2020). 3D printing of modified soybean hull fiber/polymer composites. Materials Chemistry and Physics, 254: 123452. https://doi.org/10.1016/j.matchemphys.2020.123452
[9] Sakti, A.M., Darmadi, D.B., Gapsari, F., Widodo, T.D. (2024). Physical, mechanical, and morphological characteristics of soybean fibers. Case Studies in Chemical and Environmental Engineering, 9: 100661. https://doi.org/10.1016/J.CSCEE.2024.100661
[10] Sakti, A.M., Darmadi, D.B., Gapsari, F., Widodo, T.D., Ganda, A.N.F. (2025). Enhancing the structural and antibacterial properties of soybean hull fibers via alkali treatment and zinc oxide nanocoating. Cleaner Waste Systems, 11: 100289. https://doi.org/10.1016/J.CLWAS.2025.100289
[11] Iwasaki, K.M.K., Fontana, L.C., De Medeiros, R., Becker, D. (2026). Eco-friendly surface modification to improve interfacial properties in natural fibre-reinforced epoxy composite. Journal of the Brazilian Society of Mechanical Sciences and Engineering, 48: 599. https://doi.org/10.1007/s40430-026-06552-x
[12] Ru, S.F., Zhao, C., Yang, S.M., Liang, D. (2022). Effect of coir fiber surface treatment on interfacial properties of reinforced epoxy resin composites. Polymers, 14(17): 3488. https://doi.org/10.3390/polym14173488
[13] Alvarez Marin, L., Naghizadeh Mahani, Z., Peresin, M.S. (2025). Comparative study of bleached and lignin-containing cellulose nanofibrils as reinforcements in epoxy composites. Wood Science and Technology, 59: 98. https://doi.org/10.1007/s00226-025-01696-w
[14] Hatano, R., Tominaga, Y., Imai, Y., Nakano, K. (2025). Preparation process for biomass nanofiber/bisphenol A-type epoxy resin composites with superior mechanical and thermal properties. Cellulose, 32: 3189-3206. https://doi.org/10.1007/s10570-025-06455-5
[15] Muthukumar, S., Dilip Raja, N., Raja, K., Venkatasudhahar, M. (2026). Mechanical, thermal conductivity, and water absorption properties of maguey fiber and passion fruit husk cellulose-reinforced epoxy bio composite. Silicon, 18: 521-533. https://doi.org/10.1007/s12633-025-03552-9
[16] Pham, K.A., Harris, T.A.L., Moon, R.J., Kalaitzidou, K. (2026). Functionalized cellulose nanocrystal sizing to enhance mechanical properties of glass fiber-reinforced epoxy laminates. Polymer Composites, 47: 556-567. https://doi.org/10.1002/pc.70166
[17] Gunarti, M.R., Prawoto, A., Fauzi, W.N., Wirawan, W.A. (2024). Mechanical behavior of glass fiber-epoxy composite laminates for ship hull structures. Mechanical Engineering for Society and Industry, 4(2): 156-166. https://doi.org/10.31603/mesi.11589
[18] Sulistyo, A.B., Wirawan, W.A. (2024). Evaluation of tensile strength and flexural strength of GFRP composites in different types of matrix polymers. Journal of Achievements in Materials and Manufacturing Engineering, 123(2): 49-57. https://doi.org/10.5604/01.3001.0054.6847
[19] Wang, X.L., Li, H.J., Camilleri, D., et al. (2025). Analysis of interfacial properties in flax yarn-reinforced epoxy resin composites. Fibers, 13(9): 118. https://doi.org/10.3390/fib13090118
[20] Rachtanapun, P., Sawangrat, C., Kanthiya, T., et al. (2024). Effect of plasma treatment on bamboo fiber-reinforced epoxy composites. Polymers, 16(7): 938. https://doi.org/10.3390/polym16070938
[21] Pasquali, M., De Gendt, S., Armini, S. (2021). Understanding the impact of Cu surface pre-treatment on Octadecanethiol-derived self-assembled monolayer as a mask for area-selective deposition. Applied Surface Science, 540: 148307. https://doi.org/10.1016/J.APSUSC.2020.148307
[22] Lin, T.C., Chang, J.S., Lee, D.J. (2023). Hydrophobic cotton fabric with 3-mercaptopropyltriethoxysilane/polyhedral oligomeric silsesquioxane/1-octadecanethiol modification for oil/water separation. International Journal of Biological Macromolecules, 253: 126748. https://doi.org/10.1016/j.ijbiomac.2023.126748
[23] ASTM International. (2025). ASTM D3039/D3039M-17(2025): Standard Test Method for Tensile Properties of Polymer Matrix Composite Materials. ASTM International. https://doi.org/10.1520/D3039_D3039M-17R25
[24] ASTM International. (2025). ASTM D790-25: Standard Test Methods for Flexural Properties of Unreinforced and Reinforced Plastics and Electrical Insulating Materials. ASTM International. https://doi.org/10.1520/D0790-25
[25] ASTM International. (2021). ASTM D2240-15(2021): Standard Test Method for Rubber Property—Durometer Hardness. ASTM International. https://doi.org/10.1520/D2240-15R21
[26] ASTM International. (2026). ASTM D6110-26: Standard Test Method for Determining the Charpy Impact Resistance of Notched Specimens of Plastics. ASTM International. https://doi.org/10.1520/D6110-26
[27] ASTM International. (2022). ASTM D7334-08(2022): Standard practice for surface wettability of coatings, substrates and pigments by advancing contact angle measurement. ASTM International. https://doi.org/10.1520/D7334-08R22
[28] Sulistyo, A.B., Wirawan, W.A., Muslimin, M. (2024). Evaluation of mechanical and morphological properties composite of Agel Leaf Fiber (ALF)-epoxy modified with carbon powder. EUREKA: Physics and Engineering, (1): 144-153. https://doi.org/10.21303/2461-4262.2024.002974
[29] Seid, A.M., Adimass, S.A. (2024). Review on the impact behavior of natural fiber epoxy based composites. Heliyon, 10(20): e39116. https://doi.org/10.1016/J.HELIYON.2024.E39116
[30] Aman, M., Kumar, V., Yadav, R.K., Singh, M.K. (2026). Fabrication and characterization of moonj fibre-reinforced epoxy-based composites: Tensile, flexural, hardness, and microstructural behaviours. Proceedings of the Institution of Mechanical Engineers, Part C: Journal of Mechanical Engineering Science, 240(13): 4712-4723. https://doi.org/10.1177/09544062261435222
[31] Madhu, M.G., Buddha, K. (2025). Mechanical evaluation of epoxy polymer composites reinforced with areca leaf sheath fiber. ACS Omega, 10(24): 25663-25674. https://doi.org/10.1021/acsomega.5c01365
[32] Schellbach, S.L., Monteiro, S.N., Drelich, J.W. (2016). A novel method for contact angle measurements on natural fibers. Materials Letters, 164: 599-604. https://doi.org/10.1016/j.matlet.2015.11.039
[33] Zhang, X., Wang, Y., Sun, G., Li, Y. (2026). Effect of hydrophobic modification of cellulose on the mechanical

properties of cellulose epoxy resin composites. Waste and Biomass Valorization. https://doi.org/10.1007/s12649-026-03629-5

[34] Verma, D., Gupta, D., Jawaid, M., et al. (2026). Integration of cellulosic bhimal/nettle fibers and nanofillers into epoxy-based composites: Mechanical, thermal and morphological evaluation with Weibull statistical analysis. International Journal of Biological Macromolecules, 339(2): 149824. https://doi.org/10.1016/j.ijbiomac.2025.149824

[35] Tharanitharan, G., Saravanan, C., Raja, P., Ajaykarthik, R.T. (2025). Investigation of temperature and water aging effects on epoxy composites reinforced with natural fibers and surface-modified cellulose filler. Polymer Bulletin, 82: 4621-4647. https://doi.org/10.1007/s00289-025-05682-x